ON THE DYNAMIC EFFECTS OF WHEEL RUNNING ON DISCRETELY SUPPORTED RAIL

Traian MAZILU

University *Politehnica* of Bucharest, Department of Railway Vehicles, E-mail: `trmazilu@yahoo.com`

This paper deals with the investigation of the dynamic effects of a wheel running on a rail due to parametric excitation of the discrete support. To this end, an improved track model which includes the coupling between the bending and longitudinal dynamics of the rail is utilised. In order to perform the time-domain analysis, the Green's functions method is employed. This method is based on the properties of the track as a periodic and self-damped structure, and starting from these properties the track's Green matrix is calculated and used to simulate wheel/rail interaction. The wheel/rail steady-state interaction exhibits parametric resonance and sub-harmonic resonances. The wheel/corrugated rail interaction is simulated. The study points to influence of the nonlinearities of the wheel/rail contact, i.e. the characteristic of the Hertzian contact, the geometric nonlinearity due to the effect of the wheel radius on the wheel/rail relative displacement, and the contact loss.

Key words: wheel/rail interaction, ballasted track, corrugation, Green's functions.

1. INTRODUCTION

Predicting the wheel/rail interaction is crucial to study some practical problems such as generation of rolling noise [1], growth of the rail roughness and formation of rail corrugation [2]. The starting point of these phenomena is the wheel/rail vibration which is caused especially by the defects of the rolling surfaces and the parametric excitation due to varying dynamic stiffness induced by the sleepers.

In the models most commonly used it is assumed that the two rails vibrate independently due to flexibility of the sleepers. For this reason, a single rail is considered. This rail is modelled as a uniform Euler [3], or Timoshenko [4] beam with elastic and discrete supports including the mass of the sleepers. When the wavelength of the bending wave approaches to the span length, the Euler beam model fails and has to be substituted by the Timoshenko beam model. Despite of this improvement, the vibration level of the rail at the resonance due to discrete support is systematically overestimated. To overcome this shortcoming, the rail model has to take into account that the bending and longitudinal dynamics are coupled due to rail pad [5].

The modelling of the wheel/rail interaction may be solved using either the model of a moving irregularity between a stationary wheel and rail, or the model of a moving wheel along the rail. The model of the moving irregularity is much easier to use and is utilized for the frequency-domain analysis, but it is not able to introduce the parametric excitation due to sleepers.

The model of the moving wheel is more realistic, but raises certain difficulties when it is applied. One of these is related by the contradiction between the infinite length of the track and the finite length of the model used for the time-domain analysis. In fact, the truncated model inserts the wave reflections and affects the periodic feature of the track. To surmount these undesirable effects, the truncated model of the track must include lots of sleepers, which is time consuming. Many practical solutions have been suggested: the *cutting and merging* method [6], the equivalent parametric model [4] and the Fourier-series approach [7].

However, which one of these methods is applied, it is mandatory to take some cautions. For instance, in the case of the equivalent parametric model, the rail response at the pinned-pinned frequency is not so accurate [8]. Besides, this approach may replace a propagating vibration mode with a non-propagating one, or vice versa, like the moving irregularity approach. On the other hand, the Fourier-series approach starts from the assumptions that wheel/rail system is linear and the rail head roughness is periodic and its period is

multiple or sub-multiple of the sleeper bays.

In order to avoid the previous difficulties and restrictions, the Green's functions method may be used [9], [10]. This method is based on the properties of the track which is self-damping structure and periodic as well. Obviously, the rail's Green functions have the same properties and all these function are numeric assembled in so-called the track's Green matrix. This matrix solves the issue of simulating the dynamic of the wheel/rail system for any rail length.

In the following, using the Green's functions method, the wheel/rail steady-state interaction will be investigated, and the dynamic effects from the corrugated rail including the contact nonlinearity due to wheel curve, as well.

2. MECHANICAL MODEL

The wheel/rail model is presented in fig. 2.1. The wheel is assumed as a loaded rigid disc which rolls without slip along the rail at a constant V speed. Wheel mass is M_w and its radius is R. The wheel is subjected to static load Q_0 and the normal contact force $Q(t)$, where t stands for time.

1. rail; 2. sleeper; 3. rail-pad; 4. ballast; 5. wheel; 6. stiffness contact.

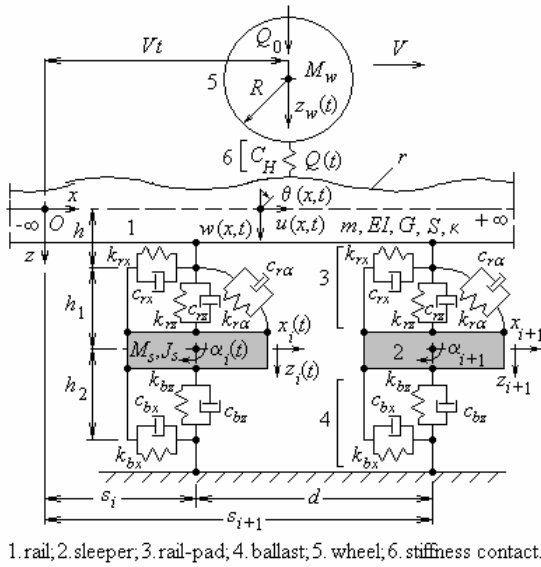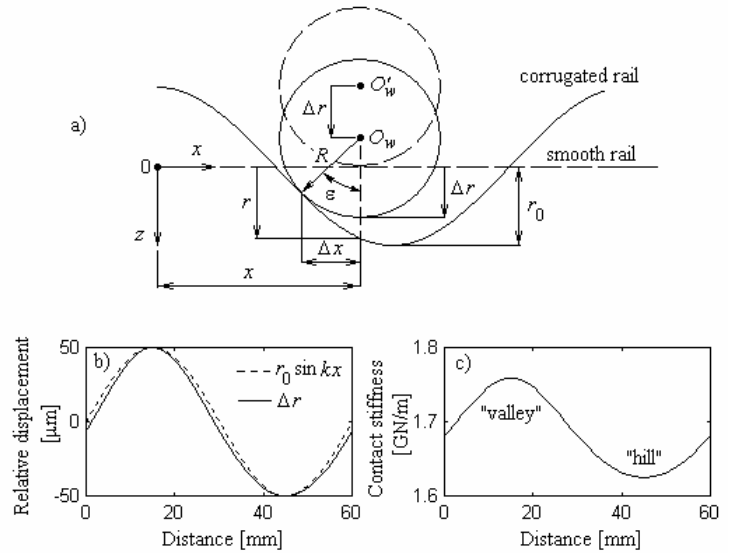Fig. 2.1.   Fig. 2.2.

This simple wheel model is motivated by the natural frequencies of the primary suspensions vehicles suspension which are significantly lower than the ones of the wheel/rail vibration.

The rail is modelled as a Timoshenko beam resting on an infinite number of equally spaced semi-sleepers via rail-pads. For longitudinal dynamics, the rail is assimilated as an infinite simple bar. The vertical and longitudinal dynamics of the rail are coupled to the rail-pads. The parameters for the rail are: the Young's modulus E, the shear modulus G, the mass per length unit m, the density ρ, the cross-section area S, the area moment of inertia I and the shear coefficient κ. The distance from the cross-section neutral fibre to the rail foot is h. The loss factor of the rail is neglected. The dynamics of the rail are: the vertical displacement $w(x, t)$, the rotation of the cross-section $\theta(x, t)$ and the longitudinal displacement $u(x, t)$.

The rail pad has 3 Kelvin-Voigt systems, 2 for the longitudinal and vertical displacements and the 3rd for the rotation in vertical-longitudinal plane. The elastic constants are k_{rx}, k_{rz} and $k_{r\alpha}$, and the viscous damping constants are c_{rx}, c_{rz} and $c_{r\alpha}$.

The ballast has 2 Kelvin-Voigt systems for the longitudinal and vertical displacements. The elastic constants are k_{bx} and k_{bz}, and the viscous damping constants are c_{bx} and c_{bz}.

The semi-sleeper is taken as a rigid body with three degrees of freedom: the vertical translation $z_i(t)$, the lateral translation $x_i(t)$ (along the rail) and the rotation $\alpha_i(x, t)$ (across the rail). The parameters for the discrete support of the sleepers are: the semi-sleeper mass M_s, the semi-sleeper mass moment of inertia J_s, the distance between the semi-sleeper i and the static frame s_i, the sleeper bay d and the distances between the semi-sleeper and the two elastic layers (modelling the rail pad and the ballast) h_1 and h_2.

With these assumptions, the governing equations of motion may be written as follows.

- The equation of motion of the wheel

$$M_w \ddot{z}_w(t) = Q_0 - Q(t), \tag{2.1}$$

where $z_w(t)$ is the vertical displacement of the wheel.

- The equations for the rail and the semi-sleepers motions

$$\mathbf{L}_{x,t}\{\mathbf{q}(x,t)\} + \sum_{i=-\infty}^{\infty}\left(\mathbf{A}_t\{\mathbf{q}(s_i,t)\} + \mathbf{B}_t\{\mathbf{q}_i^s(t)\}\right)\delta(x - s_i) = \{\mathbf{Q}(x,t)\}, \tag{2.2}$$

$$\mathbf{C}_t\{\mathbf{q}_i^s(t)\} = \mathbf{D}_t\{\mathbf{q}(s_i,t)\}$$

where $\{\mathbf{q}(x, t)\} = [u(x, t)\ w(x, t)\ \theta(x, t)]^T$ is the column vector of the rail displacements, $\{\mathbf{q}_i^s(t)\} = [x_i(t)\ z_i(t)\ \alpha_i(t)]^T$ is the column vector of the considered i sleeper displacements, $\{\mathbf{Q}(x, t)\} = [0\ {-Q(t)}\delta(x - Vt)\ 0]^T$ is the column vector of the vertical forces which act on the rail, with $\delta(.)$ is Dirac's delta function, and $\mathbf{L}_{x,t}$, $\mathbf{A}_t$, $\mathbf{B}_t$, $\mathbf{C}_t$ and $\mathbf{D}_t$ stand for matrix differential operators (see Appendix [9]).

The connection between the wheel and the rail is described by the equation of wheel/rail normal force. According to the non-linear Hertz theory, one reads

$$\left(Q(t)/C_H\right)^{2/3} = \left(z_w(t) - w_r(Vt,t) - \Delta r(Vt)\right)\sigma\left(z_w(t) - w_r(Vt,t) - \Delta r(Vt)\right), \tag{2.3}$$

where C_H represents the Hertzian constant, $\sigma[.]$ is the Heaviside function and $\Delta r(Vt)$ is the relative wheel/rail displacement due to the rail roughness (fig. 2.2 a). When the ratio between the amplitude and wavelength of rail roughness is much less than unity, and as a consequence, the ratio between the wheel radius and the curvature radius of the rail longitudinal profile is much less than unity as well, the relative wheel/rail displacement equals the rail roughness and practically the Hertzian constant has no variation.

However, these assumptions are not valid for the case of the short pitch corrugation rail [11]. Considering the corrugation as a sinusoidal form, $r = r_0 \sin kx$, where r_0 is the amplitude and k is the wave number, the wheel/rail relative displacement due to corrugation is

$$\Delta r = r_0 \sin k(x - \Delta x) + R(1 - \cos \varepsilon), \tag{2.4}$$

where ε is the contact angle and Δx is the longitudinal displacement of the contact point.

For instance, fig. 2.2b displays the relative wheel/rail displacement for the particular case of a moving wheel ($R = 460$ mm) on a sinusoidal corrugation with the wavelength of 60 mm and the amplitude of 50 μm. The difference between the rail roughness and the relative wheel/rail displacement has maximum value of 6.27 μm. According to the wheel/rail geometric contact, the contact stiffness is higher at the "valley" and lower at the "hill" as may be seen from fig. 2.2c, where the static load has been taken 100 kN. In order to simulate this effect, the Hertzian constant C_H has to be calculated for every step of the numerical integration.

In fact, the relative wheel/rail displacement due to the roughness may be taken as *the equivalent roughness,* including the wheel curve effect and the quantity $w(Vt, t) + \Delta r(Vt)$ may be seen as *the virtual position of the rail head*. Obviously, when the condition $w(Vt, t) + \Delta r(Vt) > z_w(t)$ is fulfilled, the wheel/rail contact is lost.

The mathematical model is completed by the boundary conditions

$$\lim_{|x-Vt|\to\infty}\{\mathbf{q}(x,t)\} = [0\ 0\ 0]^T, \quad \lim_{i\to\pm\infty}\{\mathbf{q}_i^s(t)\} = [0\ 0\ 0]^T \tag{2.5}$$

and the initial conditions which are set null.

3. NUMERICAL APPLICATION

In this section, both frequency-domain and time-domain numerical analysis of a particular wheel that uniformly moves along a discretely supported UIC 60 rail is presented. Notice that the moving irregularities model is used in order to perform the frequency-domain analysis.

The parameters for the rail are: m = 60 kg/m, E = 210 GPa, G = 80.8 GPa, κ = 0.4, ρ = 7850 kg/m^3, S = 7.69· 10^{-3} m^2 and I = 30.55·10^{-6} m^4. The parameters for the discrete support are chosen as follows: M_s = 129 kg, I_s = 1.28 kgm^2, d = 0.6, h = 0.08 m , h_1 = 0.116 m, h_2 = 0.114 m, k_{rx} = 50 MN/m, k_{rz} = 240 MN/m, $k_{r\alpha} = k_{rz}c^2$ /3 = 512 kNm/rad ($2c$ = 160 mm, rail pad width), c_{rx} = 10 kNs/m, c_{rz} = 55.8 kNs/m, $c_{r\alpha} = c_{rz}c^2/3$ = 119 Nms/rad, k_{bx} = 39.6 MN/m, k_{bz}= 42 MN/m, c_{bx} = 52 kNs/m, and c_{bz} = 44.2 kNs/m. The parameters relating to the wheel are: M_w = 750 kg, R = 0.46 m and Q_0 = 100 kN. Finally, the wheel has the S 78 rolling profile (used at CFR).

For the numerical simulation, the track model length of 40 sleeper bays has been considered in order to preserve the periodic feature of the track along of 10-12 sleeper bays in the central zone of the model.
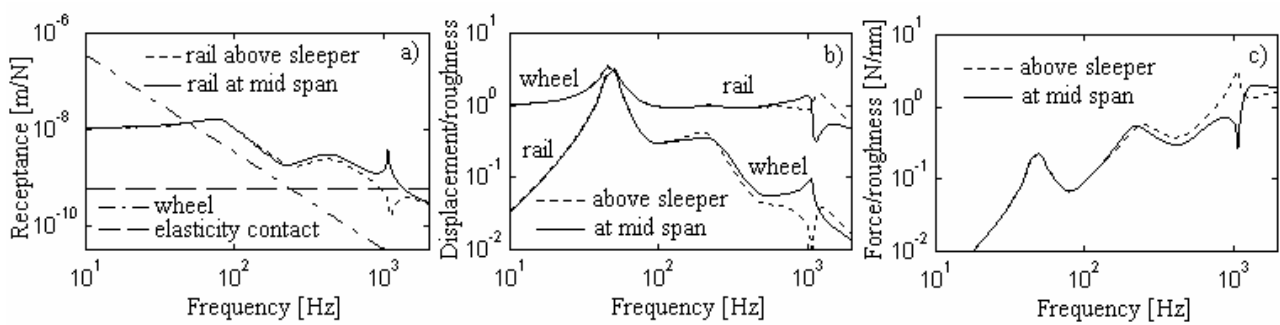

Fig. 3.1.

The dynamic behaviour of the wheel/rail system is depended by the receptances of the wheel and rail, and the contact elasticity as well (fig. 3.1a). The rail's receptance is dominated by two resonance frequencies at about 73 Hz and 436 Hz because the rail and the sleepers vibrate like a system with 2 d.o.f.s.. Also, the rail's behaviour exhibits an anti-resonance frequency which appears at approximately 240 Hz due to the vibration absorber effect given by the sleeper. At frequencies lower than the anti-resonance frequency, the rail vibrates uniformly either at mid span or above sleepers. Substantial differences may be identified at higher frequencies when the rail is more sensitive between sleepers. At high frequency, the dynamic response of rail is dominated by the effect of the periodic support, which is made by the sleepers from the rail is fixed. This effect is strongly linked to the position of excitation force. In case of excitation between the sleepers, the rail is resonant like a beam on two supports and the vertical bending wavelength equals twice the span. This resonance is so-called "pinned-pinned resonance" and it appears around 1075 Hz. If the excitation force is applied above sleeper, the rail dynamics exhibits an anti-resonance behaviour at a frequency slightly higher than the pinned-pinned resonance one, which is 1120 Hz for the analyzed case. The rail's receptance diagram is consistent with the results from the previous experimental and theoretical researches which have been developed in this topic [4], [7], [8], [12].

The wheel and rail receptances meet at about 48 Hz. At lower frequencies, the wheel's receptance is higher than the rail's and beyond this frequency the ratio reverses due to the wheel inertia. The contact elasticity is significantly lower than the rail receptance, but the difference between them decreases as the frequency increases. Finally, the 2 receptances intersect at higher frequencies around 1000 Hz, in the pinned-pinned resonance/anti-resonance zone.

The wheel/rail displacements are presented in fig. 3.1b, and the wheel/rail contact force in fig. 3.1c. All sizes are compared to roughness. As it may be observed, the wheel/rail system exhibits 2 resonance frequencies, one at 48 Hz, and the other at 240 Hz. The first resonance frequency corresponds to the own frequency of the wheel on track. At frequencies below the first resonance frequency, the wheel displacement is higher than the rail's because the rail receptance is smaller (the rail is rigid), and then the bias changes. The second resonance frequency appears when the sleeper plays as a dynamic absorber for the rail.

On the other hand, it is easy to notice the difference between the system's response above a sleeper and at mid-span. This difference reaches its magnitude at the pinned-pinned resonance/anti-resonance frequencies. In this range, the rail resonance entails the wheel anti-resonance and the rail anti-resonance determines the wheel resonance. Also, the contact force is higher above sleeper and lower at mid span because the track elasticity increases from sleeper towards the mid span.
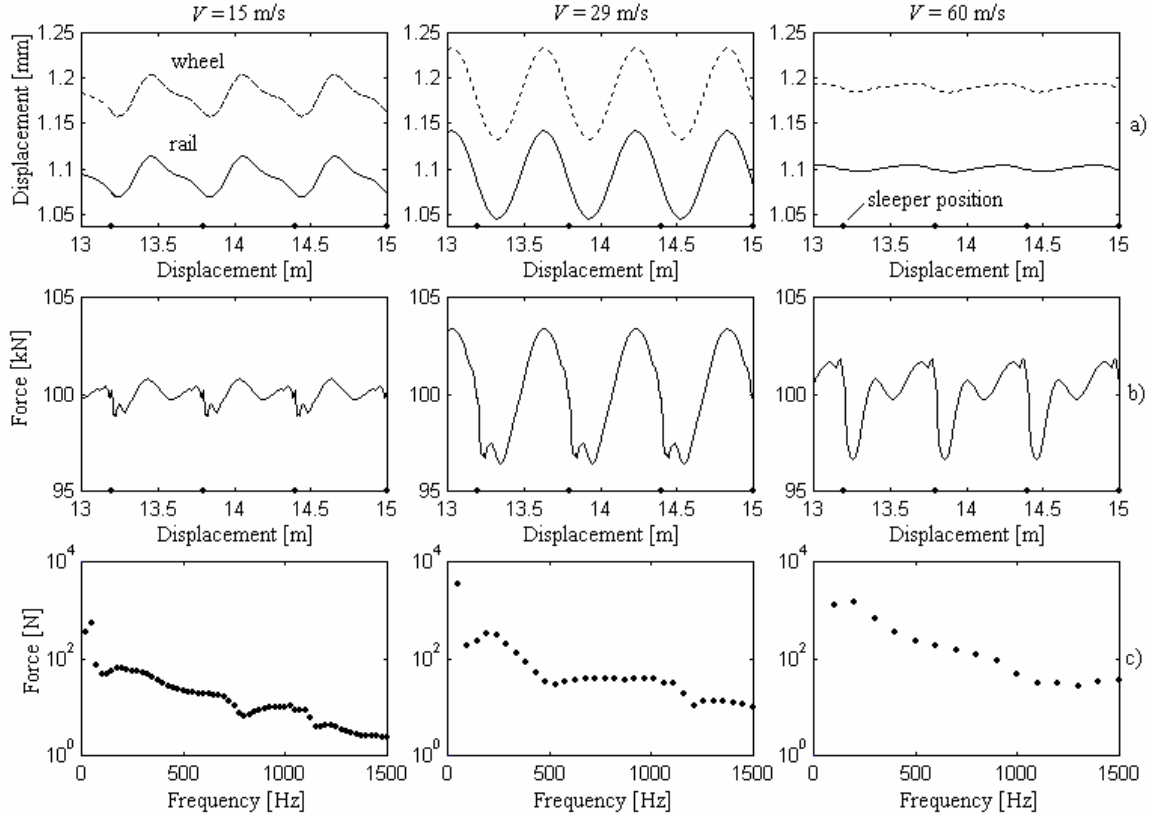

Fig. 3.2.

In the following, the numeric simulation results in the time-domain are analyzed using the Green functions method which has been presented in [9], [10]. The track Green matrix was calculated for many speed values between 8 and 80 m/s. To this end, the rail's complex Green functions have been integrated between 0 and 2872 Hz (the second pinned-pinned resonance frequency) with the integration step of 8 Hz. In order to capture the high frequency dynamic response, the time step for integrating the equations of motion was chosen between 12.5 μm and 62.5 μm. More precisely, the sample step was 0.5 mm for the speeds below 16 m/s, and 1.0 mm for the rest.

Fig. 3.2a shows the wheel/rail displacements at the contact point for the steady-state behaviour (the case of the smooth rail) between sleepers # 22 and # 25, for different speeds. The dynamics is periodic due to the periodicity of the track along the running direction. The frequency of passing over sleepers, named as the frequency of the parametric excitation, is given by the ratio between the wheel velocity and the sleeper bay.

The wheel and rail displacements are similar, but the wheel displacement is higher than the rail's due to elasticity of the contact. The minimal displacements are recorded above the sleepers at the speed of 15 m/s. At higher speeds, the minimal displacements occur after the wheel passes over the sleepers. At the wheel speed of 29 m/s, the frequency of passing over sleepers equals the first resonance frequency, and this fact counts for the magnitude of displacements – the parametric resonance. On the other hand, when the wheel speed has the value of 15 m/s, the 2nd spectral component of wheel/rail interaction due to parametric excitation equals practically the 1st resonance frequency. As a consequence, the motion presents the tendency to have a double oscillation along the sleeper bay. If the speed exceeds the value corresponding to the parametric resonance, then the wheel/rail displacements decrease as the speed increases.

The time histories of the wheel/rail contact force for the previous speeds and the corresponding spectra are displayed in fig. 3.2.b. The contact force is minimal above the sleeper which shows the natural wheel's proclivity to take off (see the preceding figure). Additionally, the highest variation of contact force occurs in sleepers' zone and this aspect may be related by the formation of rail corrugation which starts especially from the sleepers.

The spectra were calculated on a single period (fig. 3.2c). The frequencies of the harmonic components are multiples of the fundamental frequency (the frequency of the parametric excitation). As a general rule, the spectrum is dominated by the first component which has the frequency of parametric excitation. However, at the speed of 15 m/s the 2nd spectral component is higher (1.56 times) than the fundamental component because it is augmented by the 1st resonance of wheel/rail system. Also, at the speed of 60 m/s, the 2nd spectral component has 200 Hz and it is situated close to the 2nd resonance. For this reason, it is amplified and dominates the spectrum of the contact force (1.15 times of the fundamental component).

The spectra remind of the shape of the frequency response of the wheel/rail system, but they play as a cut-off filter. Despite of this aspect, as the wheel velocity increases, the power of the spectral components situated in the pinned-pinned resonance range increases.

The diagram of the effective contact force versus the wheel velocity is plotted in fig. 3.3. The very clear parametric resonance behaviour at the speed of 29 m/s is exhibited. Also, one may be observed the effect of the ½ sub-harmonic parametric resonance at speed of 14-15 m/s. Even the weak trace of the ⅓ sub-harmonic resonance around the speed of 10 m/s may be seen. In this case, the 3rd spectral component is amplified by the main resonance of the wheel/rail system. Similar sub-harmonic parametric resonances have been studied in the case of the pantograph-catenary system.

When the wheel rolls on a rail with irregularities, 2 types of excitation, the parametric excitation and the excitation due to the irregularities, are overlapped, and the result is an amplitude-modulated vibration. In order to fix the ideas, let consider the case of corrugated rail which may be modelled as a sinusoidal function.
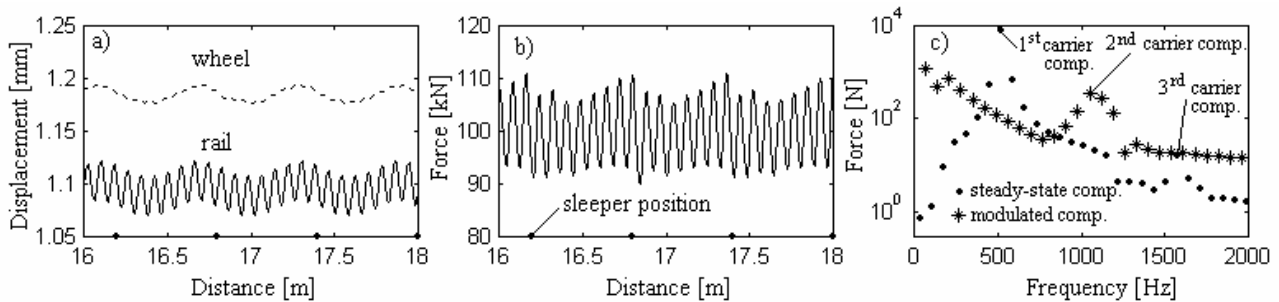
Fig. 3.4. shows the numeric results from a wheel moving at 42 m/s over a sinusoidal roughness which has a wavelength of 80 mm and the amplitude of 20 μm. The modulated vibration has the carrier frequency of 525 Hz which correspond to wheel velocity and roughness wavelength, and the modulation frequency of 70 Hz (the fundamental component) which is given by the parametric excitation due to the sleepers. In fact, the motion is periodic with the period of 1.2/42 s which corresponds to the frequency of 35 Hz.

The wheel amplitude is much smaller than the rail's amplitude at the considered contact point. This aspect is consistent with the results from the frequency-domain analysis. The time history of the contact force shows a better understanding of the modulated vibration character. The spectrum of the contact force has 2 kinds of components, from the parametric excitation and from the carrier with the modulated components. Actually, the vibration is non-linear due to wheel/rail contact including the Hertz's contact effect and the influence of radius wheel, and the carrier has many harmonic components with the frequencies of kf_c where f_c stands for the carrier frequency and k stands for an integer number. The modulated spectral components have the frequencies of $kf_c \pm pf_0$, where f_0 stands for the frequency of the parametric excitation

and *p* stands for an other integer number. The 2 kinds of spectral components may overlap or not. For the analyzed case, the spectral component due to parametric excitation are not overlapped on the modulated spectral components given by the carrier or by the 3rd carrier component, but they are overlapped on the modulated spectral components given by the 2nd carrier component. The explanation is simple, the frequency of the 2nd carrier component is multiples of the frequency of the parametric excitation and the frequencies of the other components are not.

The influence of the geometric nonlinearity due to wheel radius is of importance from theoretic point of view. To this end, the contact force spectra have been calculated for both hypotheses, once the wheel radius is ignored and the wheel/rail relative displacement due to rail roughness is given by the roughness only, respectively the case of the equivalent roughness. The ratio between the spectral components from the 2 numeric simulations is displayed in

Fig. 3.5.

figure 3.5. The wheel radius has no significant influence, excepting the frequencies of harmonic components of the carrier. For the particular case which is discussed here, the 2nd carrier component falls in the pinned-pinned resonance range and the modulated spectral components are very sensitive to the geometric nonlinearity due to wheel radius.
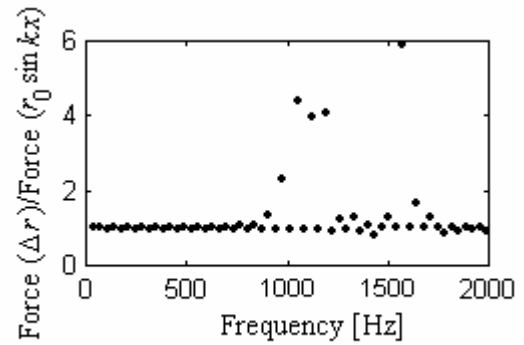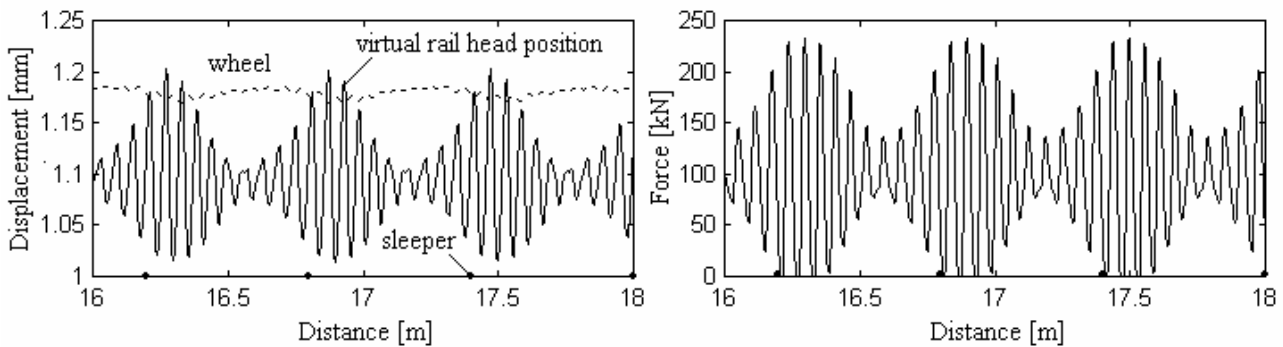

Fig. 3.6.

Rolling on the corrugated rail, the dynamic effects increase especially when the vibration frequency is placed in the pinned-pinned resonance domain. Fig. 3.6 presents the results from the numerical simulation that consider a wheel rolling at 64 m/s over a sinusoidal irregularitie which have the wavelength of 60 mm and the amplitude of 70 μm. The wheel vibration has very low level due to its inertia, and practically the rail vibrates only and compensates the corrugation by its displacement. The contact force has high variations around the static load value. This variations increase as the corrugation amplitude increases so that even the contact may be lost as may be observed.

The influence of the corrugation amplitude on the contact force is shown in fig. 4.10. The maximum and minimum values of the contact force are displayed and the effective contact force as well. The maximum and effective values of the contact force have a linear increase,

Fig. 3.7.

meanwhile the minimum contact force decreases linearly. When the contact is lost, both maximum and effective values of the contact force increase linearly as well, but their increase lowers.
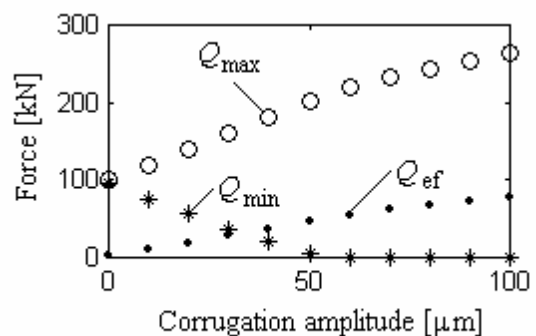
6. CONCLUSIONS

In this paper, the dynamic effects of a wheel running on a discretely supported rail were investigated using an improved model which takes into account the coupling between the bending and longitudinal dynamics of the rail. To this end, the rail was modelled as an infinite Timoshenko beam and a bar resting on semi-sleepers via rail pads with 3 directions. The time domain analysis was performed utilising the real Green functions method. Basing on the properties of the track which is periodic and self-damping structure, the track's Green matrix has been calculated. Then, this matrix was helpful to simulate the dynamic interaction between a moving wheel and rail, including the nonlinearities of the wheel/rail contact.

The wheel/rail system shares the same properties with a parametric system and its steady-state interaction exhibits multiple resonances. The main parametric resonance occurs when the frequency of the parametric excitation due to sleepers equals the own frequency. Also, the ½ and ⅓ sub-harmonic parametric resonance may be recorded when the wheel velocity equals ½ and ⅓ respectively of the value corresponding to the velocity of main parametric resonance. The spectra of wheel/rail contact force are influenced by the wheel velocity by pushing the powerful components at high frequency as the speed increases. As a consequence, the vibration level increases encouraging the formation of the corrugated rail.

If the wheel rolls on a corrugated rail, the wheel/rail vibration becomes amplitude modulated. The carrier has many harmonics due to nonlinearities of the contact. For some conditions, the spectral components may be overlapped increasing the vibration level. The 2nd and 3rd carrier components are very sensitive to the geometric nonlinearity due to the influence of the wheel radius on the wheel/rail relative displacement. Also, running on the corrugated rail induces strong dynamic surcharges which may affect the track structure.

ACKNOWLEDGEMENTS

REFERENCES

1. THOMPSON, D. J., JONES, C. J. C., A review of the modelling of wheel/rail noise generation, Journal of Sound and Vibration, 231, pp. 519-536, 2000.
2. SHENG, X., THOMPSON, D. J., JONES, C. J. C., XIE, G., IWNICKI, S. D., ALLEN, P., HSU, S. S., Simulation of roughness initiation and growth on railway rails, Journal of Sound and Vibration, 293, pp. 829-829, 2006.
3. CLARK, R. A., DEAN, P. A., ELKINS, J. A., NEWTON, S. G., An investigation into the dynamic effects of railway vehicles running on corrugated rails, Jorunal Mechanical Engineering Science, Vol. 24 No 2, pp. 65-76, 1982.
4. WU, T. X., THOMPSON, D. J., On the parametric excitation of the wheel/track system, Journal of Sound and Vibration 278, pp.725-747, 2004.
5. MAZILU, Tr., Propagation of harmonic vertical waves in a rail, Scientific Bulletin Series D: Mechanical Engineering, vol. 67 no. 2, pp. 99-110, 2005.
6. HOU, K., KALOUSEK, J., DONG, R. G., A dynamic model for an asymmetrical vehicle/train system, Journal of Sound and Vibration 267 pp. 591-604, 2003.
7. SHENG, X., LI, M., JONES, C. J. C., THOMPSON, D. J., Using the Fourier-series approach to study interactions between moving wheels and a periodically supported rail, Journal of Sound and Vibration 303, pp. 873-894, 2007.
8. SHENG, X., JONES, C. J. C., THOMPSON, D. J., Responses of infinite periodic structures to moving or stationary harmonic loads, Journal of Sound and Vibration 282, pp. 125-149, 2004.
9. MAZILU, Tr., Green's functions for analysis of dynamic response of wheel-rail to vertical excitation, Journal of Sound and Vibration, 306, pp. 31-58, 2007.
10. MAZILU, Tr., Wheel-rail vibrations (in Roumanian), MatrixRom, 436 pages, 2008.
11. BOGACZ, R., KOWALSKA, Z., Computer simulation of the interaction between a wheel and a corrugated rail, Eur. J. Mech. A/Solids 20, pp. 673-684, 2001.
12. THOMPSON, D. J., HEMSWORTH, B., VINCENT, N., Experimental validation of the TWINS prediction program for rolling noise, Part 1: Description of the model and method, Journal of Sound and Vibration, 193, pp. 123-135, 1996.